Quantitative assessment of nanoparticle surface hydrophobicity and its influence on pulmonary biocompatibility

Jones, Marie-Christine; Jones, S.A.; Riffo-Vasquez, Y; Spina, D; Hoffman, E; Morgan, A; Patel, A; Page, C; Forbes, B.; Dailey, L.A.

DOI:
10.1016/j.jconrel.2014.03.022

***Graphical Abstracts (for review)**

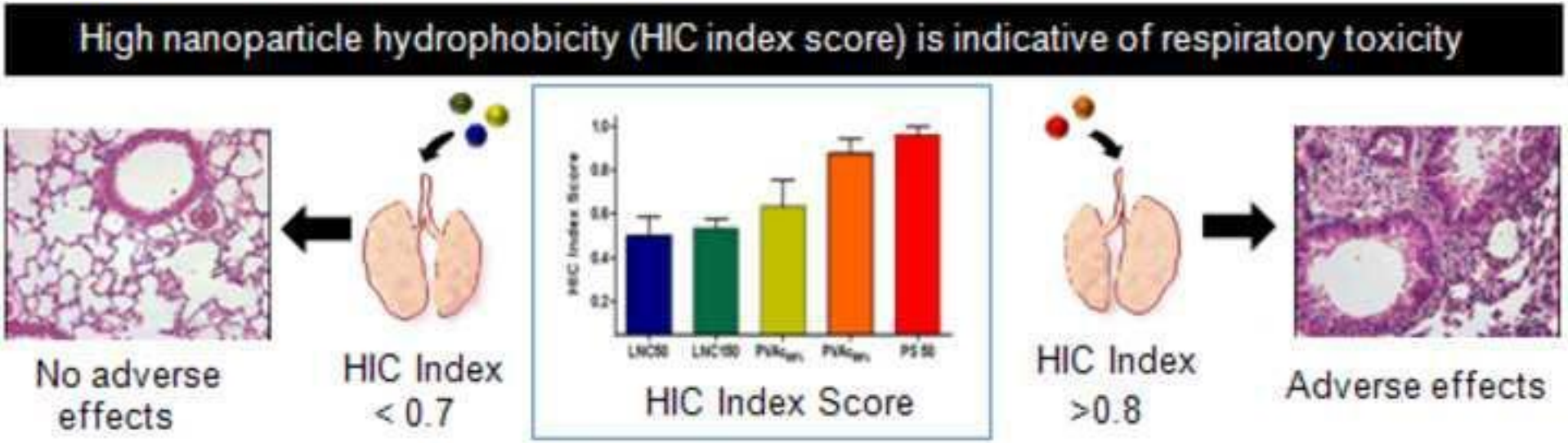

Quantitative assessment of nanoparticle surface hydrophobicity and its influence on pulmonary biocompatibility

Marie-Christine Jones[1,2], Stuart A. Jones[1], Yanira Riffo-Vasquez[1], DomenicoSpina[1], Ewelina Hoffmann[1], Anna Morgan[1], Aateka Patel[1], Clive Page[1], Ben Forbes[1], Lea Ann Dailey[1,]**

[1]Institute of Pharmaceutical Science, King's College London, 150 Stamford Street, London SE1 9NH, UK

[2]Present address: School of Clinical and Experimental Medicine, University of Birmingham, Edgbaston, Birmingham B15 2TT, UK

* Dr. B. Forbes and Dr. L.A. Dailey, Corresponding-Authors,Ben Forbes : Institute of Pharmaceutical Science, King's College London, 150 Stamford Street, London SE1 9NH, UK, Telephone: +44 207 848 4823, E-mail: ben.forbes@kcl.ac.uk. Lea Ann Dailey : Institute of Pharmaceutical Science, King's College London, 150 Stamford Street, London SE1 9NH, UK, Telephone: +44 207 848 4780, E-mail: lea_ann.dailey@kcl.ac.uk.

Abstract

To date, the role of nanoparticle surface hydrophobicity has not been investigated quantitatively in relation to pulmonary biocompatibility. A panel of nanoparticles spanning three different biomaterial types, pegylated lipid nanocapsules, polyvinyl acetate (PVAc) and polystyrene nanoparticles, were characterized for size, surface charge, and stability in biofluids. Surface hydrophobicity of five nanoparticles (50-150 nm) was quantified using hydrophobic interaction chromatography (HIC) and classified using a purpose-developed hydrophobicity scale: the HIC index, range 0.00 (hydrophilic) to 1.00 (hydrophobic). This enabled the relationship between the nanomaterial HIC index value and acute lung inflammation after pulmonary administration to mice to be investigated. The nanomaterials with low HIC index values (between 0.50-0.64) elicited little or no inflammation at low (22 cm^2) or high (220 cm^2) nanoparticle surface area doses per animal, whereas equivalent surface area doses of the two nanoparticles with high HIC index values (0.88-0.96) induced neutrophil infiltration, elevation of pro-inflammatory cytokines and adverse histopathology findings. In summary, a HIC index is reported that provides a versatile, discriminatory, and widely available measure of nanoparticle surface hydrophobicity. The avoidance of high (HIC index > ~0.8) surface hydrophobicity appears to be important for the design of safe nanomedicines for inhalation therapy.

Keywords: Nanomedicine; nanoparticles; pulmonary drug delivery; hydrophobicity, nanotoxicology; polystyrene; lipid nanocapsules

Running title: Nanomaterial hydrophobicity influences pulmonary biocompatibility

Introduction

Inhalation of drug-containing nanoscale carriers has been heralded as an important strategy for the local or systemic delivery of therapeutic agents to or via the lungs [1-5]. Inhaled nanocarriers have the potential to control drug release, prolong lung retention, target drug to specific sites in the lungs and reduce off-target side effects [6, 7]. For successful development as inhaled medicines, however, careful biomaterial design is required to avoid lung toxicity. Paradigms are emerging to link specific physicochemical properties of nanoparticles with acute lung toxicity (e.g. tissue damage, cellular influx or cytokine release) or long term adverse effects such as chronic inflammation, fibrosis, or lung cancer [8-12]. For example, there is a large body of evidence relating respiratory toxicity to nanoparticle properties such as chemically reactive surfaces, including those which generate reactive oxygen species [13], highly cationic or anionic surfaces [14-16], high particle aspect ratio [17], excessive surface area exposure of inert nanomaterials [18, 19], and biopersistence in the lungs [20]. Nanomedicine design strategies which avoid or mitigate these risk factors have been shown to result in enhanced biocompatibility profiles *in vivo* [15, 21-23].

Surface hydrophobicity is often cited as an additional risk factor for nanoparticle toxicity [20, 24, 25], but is seldom, if ever, characterized during nanoparticle profiling, which typically concentrates on particle size, shape, zeta potential, crystallinity, colloidal stability, surface reactivity, and solubility/degradability [12]. The rare studies that have investigated the relationship between nanoparticle surface hydrophobicity and *in vivo* respiratory toxicity [15], appear to indicate a relationship, but have lacked a quantitative metric for hydrophobicity. Several analytical methods are available to quantify nanoparticle hydrophobicity, including small molecule adsorption assays (i.e. dyes, hydrophobic compounds, water) [26-28] and hydrophobic interaction chromatography (HIC) [29], each of which has advantages and limitations.

Methods that measure small molecule adsorption to the particle surface provide a highly information-rich characterisation of the molecular interaction forces at the particle surface. For example, Xia *et al* [24, 25] studied the adsorption profiles of 28 different small molecule probes to the surface of multi-walled carbon nanotubes and their carboxylated derivatives using solid phase microextraction gas chromatography/mass spectroscopy. Numerical data representing five descriptors (hydrophobicity, hydrogen bonding, polarity, polarizability, and lone-pair electrons) were combined into a single value, the biological surface adsorption index (BSAI) score, which was proposed for use in modelling quantitative structure-activity relationships. Although this approach is excellent for in-depth analysis of nanoparticle surfaces, its implementation as a routine screening method is limited by the complexity and prolonged duration of analysis, as well as the requirement of specialized analytical equipment.

The aims of this study were to develop HIC as a quantitative method for measuring nanoparticle surface hydrophobicity and investigate the influence of nanoparticle surface hydrophobicity on pulmonary biocompatibility. An HIC index value was developed to provide a quantitative descriptor of nanoparticle surface hydrophobicity and used to score five nanoparticle systems based on three different biomaterial types. Polystyrene (PS) nanoparticles were used as a high hydrophobicity reference nanomaterial reported to elicit an acute inflammatory response in the lung at elevated exposure doses [18, 19, 22]. Nanoparticles fabricated from two different grades of polyvinyl acetate (PVAc) were included as

representative of polymeric systems previously investigated to serve as inert reference particles in inhalation toxicology studies [30] and are also found in some aerosolized consumer products, including hairsprays [31]. Two lipid nanocapsule (LNC) formulations (nanocarriers characterized by a liquid triglyceride core and a solidified phospholipid shell containing pegylated 12-hydroxystearate) were included in the study to exemplify promising nanomedicine formulations for pulmonary delivery of poorly soluble compounds [32-36].

The nanoparticle systems included in the study were designed such that they would display a range of surface hydrophobicities. All the nanoparticles were chemically inert, amorphous, spherical with diameters of either 50 or 150 nm and had a negligible surface charge. The hypothesis of the study was that increasing nanoparticle surface hydrophobicity, as measured by HIC, would correlate with acute respiratory toxicity when administered to the lungs of mice.

Materials and Methods

Two molecular weight grades of PVAc, high (48 kDa) and low (12.8 kDa), were purchased from Sigma-Aldrich (Dorset, UK). Poly vinyl alcohol (PVA; 8-12 kDa) was purchased from Sigma-Aldrich (Dorset, UK). Labrafac® Lipophile WL1349 was obtained from Gattefosse (Saint-Priest, France), Solutol® HS15 was acquired from BASF (Ludwigshafen, Germany) and Lipoid® S75-3, from Lipoid GmbH (Ludwigshafen, Germany). Non-modified polystyrene nanoparticles with a diameter of 50 nm (2.62% m/v) were used as a reference material and were purchased from Polysciences (Eppelheim, Germany). All other materials were of analytical grade.

2.1 Nanoparticle fabrication

2.1.1 PVAc nanoparticles

To produce differential degrees of hydroxylation, the PVAc polymers were modified by direct saponification according to the method described by Chana et al [37] producing a PVAc polymer with 17 mol% hydroxyl groups and 83 mol% residual acetate groups (PVAc80%) from the high molecular weight precursor and a modified PVAc polymer with 34 mol% hydroxyl groups and 66 mol% residual acetate groups (PVAc60%) from the low molecular weight polymer. Polymer purity and degree of hydrolysis were verified by NMR analysis prior to use [37]. PVAc60% nanoparticles were prepared by injecting a solution of 5% w/v PVAc60% polymer dissolved in 2:1 methanol:water into a 0.33% w/v aqueous PVA solution, whilst stirring at 3500 rpm using a Silverson L4 homogenizer (Silverson Machines Ltd., Waterside, UK). PVAc80% nanoparticles were prepared by injecting a solution of 1% w/v PVAc80% polymer dissolved in 2:1 methanol:water into a 0.33% w/v aqueous PVA solution, whilst stirring at 3500 rpm. Following 30 min constant stirring at 4000 rpm and solvent evaporation overnight (~100 rpm), the nanosuspensions were dialyzed against water (72 h) to remove excess PVA and subsequently concentrated to the desired final concentration using ultrafiltration centrifuge tubes (100 kDa MWCO; Millipore, Watford, UK). Residual PVA was quantified colorimetrically using a method adapted from Sahoo *et al.* [38].

2.1.2 Lipid nanocapsules

LNCs were manufactured using a phase-inversion temperature method [39]. LNC with 50 nm diameters (LNC50) were prepared by generating a coarse emulsion of 17% w/w Labrafac® Lipophile WL1349, 17% w/w Solutol® HS15, and 1.75% w/w Lipoid® S75-3 in a 3% w/w NaCl solution. This emulsion was then submitted to repeated heating cooling cycles (85°, 60°, 85°, 60°, 85°C) before adjusting to 72°C. At this point the mixture was quenched in a 2-fold volume of ice water and stirred at room temperature for 5-10 min. LNC with 150 nm diameters (LNC150) were prepared and purified using a similar method, but the relative concentrations of components were: 25% w/w Labrafac® WL1349, 8.5% w/w Solutol® HS15, 1.5% w/w Lipoid® S75-3. In the final step of manufacture, the nascent LNC150 nanoparticles were diluted with 2.5 volumes of ice cold water.

Excess stabilizer (Solutol® HS15) was removed from all suspensions by dialysis (72 h) against water containing BioBeads® (BioRad, Hertfordshire, UK) and subsequent concentration using ultrafiltration centrifuge tubes (Millipore, UK; 100 kDa MWCO). Residual Solutol® HS15 was determined colorimetrically[40]. Briefly, following LNC purification by ultrafiltration (as described above), a 50 µL aliquot of the ultrafiltrate containing Solutol® HS15 was added to equal volumes (600 µL) of chloroform and an aqueous solution of ammonium ferrothiocyanate (16.2 g L^{-1} anhydrous ferric chloride; 30.4 g L^{-1} ammonium thiocyanate). The biphasic mixture was incubated under gentle stirring for 30 min at room temperature. The bottom chloroform layer was assayed spectrophotometrically at λ= 510 nm and the Solutol® HS15 content determined from a calibration curve.

2.2 Nanoparticle characterization

2.2.1 Nanoparticle size and zeta potential

Particle size and zeta potential were determined using a Zetasizer Nano ZS (Malvern, Worcestershire, UK). Size was measured at 25°C in purified water and 5% dextrose over four weeks to assess storage stability. Stability after aerosolization was assessed by aerosolizing 25 µL nanoparticles suspended in 5% m/v dextrose with a Microsprayer® device (Penn-Century Inc.; Wyndmoor, PA, USA) into 1 mL purified water at 25°C. Size stability in biological medium was assessed by aerosolizing 25 µL nanoparticles suspended in 5% m/v dextrose into HBSS containing 10% v/v FBS at 37°C and measuring particle size at t=0, 0.17, 4 and 24 h. Measurements were taken at a scattering angle of 173°. Refractive indices and viscosity values were adjusted for each temperature and medium used. While all nanoparticle suspensions were size-stable when stored in purified water at 4°C, fresh batches were prepared for each *in vivo* experiment. Zeta potential measurements were performed at 25° C with all suspensions diluted in 6.3 mM NaCl.

2.2.2. Hydrophobic interaction chromatography

Surface hydrophobicity of nanoparticle suspensions (n=3 individual batches) was

assessed using HIC [29]. Briefly, nanoparticle suspensions were prepared in PBS (~1 mg mL^{-1}) and 250 µL eluted through three different HiTrap™ substituted sepharose hydrophobic interaction columns: Butyl FF, Phenyl FF (high substitution) and Octyl FF (GE Healthcare Life Sciences, Little Chalfont, UK). The eluent was collected in 1 mL fractions and analyzed for particle content via turbidity measurement (Lambda 35;Perkin-Elmer, Cambridge, UK; λ=450 nm). Particles were subsequently eluted from the column using 0.1% Triton X-100. Absorbance values were plotted against elution volumes and two area under the curve (AUC) values were calculated using Origin™ software. The particle retention in each of the three columns was defined according to Equation (1):

$$(1)\ \%\ Column\ retention\ (\%R) = \left(\frac{AUC\ TritonX}{AUC\ PBS + AUC\ TritonX}\right) \times 100$$

The HIC index value was calculated according to Equation (2):

$$(2)\ HIC\ Index = \frac{\left(\%R_{butyl} \times \log P_{butyl}\right) + \left(\%R_{phenyl} \times \log P_{phenyl}\right) + \left(\%R_{octyl} \times \log P_{octyl}\right)}{\left(100\% \times \log P_{butyl}\right) + \left(100\% \times \log P_{phenyl}\right) + \left(100\% \times \log P_{octyl}\right)}$$

whereby, log P values of each column linker were calculated as: 0.47, 0.94 and 2.05 for butyl, phenyl and octyl modified columns, respectively. The log P values of the column linkers were calculated using Marvin Sketch (version 5.5.0.1,Chem Axon Limited). In the denominator, each log P value was multiplied by 100%, which represents the theoretical case of 100% retention on each column achieved by a particle with maximum hydrophobicity.

2.3 In vivo safety evaluation

2.3.1 *Nanoparticle dose and pulmonary administration*

Male Balb/c (6–8 weeks old, ~22-25 g; Harlan, UK) were used in acute respiratory toxicology studies utilizing a single pulmonary administration of nanoparticles. All experiments were in accordance with the U.K. Home Office regulations and approved by the King's College London research ethics committee. Nanoparticles were administered at doses of 22 cm^2 or 220 cm^2 nanoparticle surface area per animal (equivalent mass doses are listed in Table 1). The use of the surface area dose metric is supported by independent studies suggesting that nanoparticle surface area is a more robust descriptor of respiratory toxicity for biopersistent nanoparticles compared to mass or particle number dose [19, 41]. For example, it has been shown that nanoparticles of different diameters elicit an equivalent inflammatory response when administered at equal surface area doses [18, 19]. Nanoparticle surface area doses were calculated from the hydrodynamic diameter of the particles, assuming a density of ca. 1 g cm^{-3} for PVAc nanoparticles, 0.96 g cm^{-3} for LNC (estimated from the density of the main constituent, Labrafac® WL1349) and 1.05 g cm^{-3} for PS50 (manufacturer's information). It should be noted that the doses used in this study fall within the typical dose ranges used in toxicology assessments of inhaled pharmaceutical compounds when determining the 'no observed adverse effect level' values in nonclinical studies. All suspensions were prepared in sterile dextrose 5% w/v to ensure isotonicity. Vehicle controls were prepared by suspending nanoparticles in sterile dextrose 5% w/v and using ultrafiltration centrifugation (Millipore, UK; 100 kDa MWCO) to separate the vehicle from the

suspension as described above.

Isoflurane-induced anesthesia (1-3%) was maintained with intraperitoneal injection of 100 mg kg^{-1} ketamine mixed with 20 mg kg^{-1} xylazine in 0.1 mL saline to allow intratracheal dosing with the Microsprayer® aerosolizer. This combination of tranquilizer/dissociative yielded a moderate level of anesthesia for15-20 minutes, as assessed by paw pinch withdrawal reflex. Mice were suspended at a 45° angle by their upper incisors and nanosuspensions (25 μL) were administered as a coarse aerosol into the lungs using the Microsprayer® device. This device was chosen as it has been reported to provide a more homogenous distribution of liquid suspensions into murine lungs compared to intratracheal bolus injections [42]. Animals were kept warm post-treatment with a heat lamp, then returned to their cages when ambulatory (<15 min).

2.3.2. Bronchoalveolar lavage, cytology and histopathology

At 24 h after nanoparticle administration, mice were euthanized via terminal anesthesia with urethane (2 mg g^{-1} i.p.). The trachea was exposed, cannulated and the lungs were lavaged with three aliquots (0.5 mL) of sterile saline. The total number of cells in the cellular fraction of the lavage was counted with a Neubauer haemocytometer (Fisher Scientific, Loughborough, UK). Differential cell counts were performed using cytospin preparations, i.e. 100 μL BAL cellular fraction centrifuged at 300 g for 1 min using a Shandon Cytospin 2 (Shandon Southern Instruments, Sewickley, PA, USA) at room temperature. Cells were stained with Diffquick® (DADE Behring, Marburg, Germany) and a total of 200 cells were evaluated to determine the proportion of neutrophils, eosinophils and macrophages using standard morphological criteria. Eosinophils were not observed in any of the samples and are not reported. It was assumed that at the time point studied, the mononuclear cell population consisted primarily of resident alveolar macrophages and therefore lymphocyte numbers were not investigated. The alveolar macrophage population was assessed further by evaluating 100 macrophages to subcategorize their morphology as normal, finely or coarsely vacuolated.

Cytokines present in the BAL supernatant were quantified using a murine 7-plex proinflammatory cytokine assay (MSD® 96-Well Multi-Spot Cytokine Assay; Meso-Scale Discovery, Gainsborough, MD, USA) coupled with an MSD Sector Imager, which measures cytokine content via electrochemiluminesce. The cytokines analysed were: IFN-γ, IL-1β, IL-6, IL-10, IL-12p70, CLCX1, and TNF-α. The only cytokines/chemokines in the BAL samples at levels above the limit of quantification wereIL-1β, IL-6, CLCX1, and TNF-α. As a measure of tissue integrity, total protein levels in BAL were quantified using a Quick Start™ Bradford Protein Assay (Bio-Rad, Hemel Hempstead, UK) according to manufacturer's instructions.

Lung tissue histopathology was performed in a randomized, blinded study by an independent pathologist according to the Organization for Economic Co-operation and Development (OECD) guidelines for histopathology assessment in inhalation toxicity studies, [43]. Lungs were removed after terminal anesthesia, inflated with 10% formalin, then immersed in 10% formalin for at least one week prior to tissue processing. Samples were coded prior to

submission to the pathologist, who produced prepared hematoxylin and eosin (HE) stained sections and analyzed them according to OECD guidelines. Analysis was performed in five animals using five different sections per lung (across different lobes). Frequency data describe the number of animals out of five exhibiting an adverse finding, while the severity score (scale of 0-5) describes the number of positive adverse findings across the 25 tissue sections in a group divided by five.

2.4 In vitro investigations of macrophage responses

2.4.1 Culture conditions

J774 cells (derived from BALB/c mice) were used as a macrophage-like cell line. Cells were cultured at 37˚C in a 5% CO_2/95% air atmosphere. Culture media consisted of phenol red-free Dulbecco's Modified Eagle Medium (DMEM; Invitrogen, UK), supplemented with 10% v/v foetal bovine serum (FBS), 1% m/v penicillin/ streptomycin, and 2 mM L-glutamine.

2.4.2 In vitro evaluation of apoptosis and mitochondrial activity

J774 cells were seeded onto 8-well glass chamber slides (NuncLabTek II, Fisher Scientific, Loughborough, UK) at 5 x 10^4 cells per well and cultured for 24 h to allow for cell attachment. Subsequently, the cell culture medium was removed and replaced with 100 µL fresh cell culture medium containing 0.5, 1, 5, 10 mg mL^{-1} PVAc60% or PVAc80% nanoparticles. Controls were fresh cell culture medium (untreated control) or vehicle control, prepared as previously described. After 24 h, 1 µL of NucView™ 488 (caspase 3/7 substrate; Biotium Inc., Hayward, CA, USA) and MitoView™ 633 (mitochondrial dye; Biotium Inc., Hayward, CA, USA) probe solutions were added. The probes were incubated for 30 min prior to live cell imaging using a Leica DMIR E2 confocal microscope (Leica Microsystems, Milton Keynes, UK). Transmission images plus fluorescent emissions from NucView™ 488 (λ_{ex} = 488 nm; λ_{em} = 500-530 nm) and MitoView™633 (λ_{ex} = 633 nm; λ_{em} = 648 nm) were collected using separate channels at a magnification of 40x. Instrument gain and offset values were adjusted using the negative control and remained constant for all subsequent experiments. Images obtained from each scan were pseudo-colored green (NucView™ 488) and red (MitoView™633). The presented results depict a representative image from n = 3 different sections of the same well. The prevalence of apoptotic cells in the total population was determined by calculating the percentage of caspase 3/7 positive cells from the total number of cells in n=3 different images (~100 cells per image). To conduct a quantitative evaluation of mitochondrial activity, cells were seeded at the same density into 96-well plates and treated with fresh cell culture medium containing 0.5, 1, 5, 10 mg mL^{-1} PVAc60% or PVAc80% nanoparticles. Controls were fresh cell culture medium (untreated control) or vehicle control, prepared as previously described. Following 24 h incubation, the 3-(4,5-dimethythiazol-2-yl)-2,5-diphenyl tetrazolium bromide (MTT) assay was performed using a previously reported methodology [44] with the experiment repeated on two occasions with three replicates at each

concentration of test substance.

2.5 Statistical analysis

SPSS version 20 (IBM, UK) was used for all statistical analyses. HIC index analysis was performed using a one way ANOVA comparison with a post-hoc Tukey test. BAL cell counts from nanoparticle- and vehicle-challenged mice were compared by using ANOVA on log transformed data followed by the Sidak correction. Data pertaining to the different macrophage phenotypes and BAL cytokine levels were analysed using Kruskall Wallis followed by multiple distribution free post-hoc test. $P<0.05$ were considered significant and denoted as: * $p<0.05$, ** $p<0.01$, and *** $p<0.001$.

3. Results

3.1 Nanoparticle characterization

All nanoparticles possessed a narrow size distribution (Table 2) and a slightly negative to neutral zeta potential, consistent with the use of non-ionic stabilizers (e.g. polyetheylene glycol and polyvinyl alcohol) which were chosen to reduce the impact of high surface charge as a confounding factor in the toxicity studies [14]. Following manufacture, all formulations were extensively purified resulting in low levels of excess stabilizer in the vehicle (Table 2). Although the nanoparticles formed two distinct size groups (~50 and 150 nm) within the panel, this was accounted for in subsequent *in vivo* studies by administration of equivalent surface area doses [19, 41].

Surface hydrophobicity was quantified by HIC using three different column chemistries to enhance the discriminatory power of the method (Figure 1a). HIC index values were calculated on a scale ranging from 0.00 (maximum theoretical hydrophilicity) to 1.00 (maximum theoretical hydrophobicity). The nanoparticle panel spanned the upper 50% of the HIC scale with values ranging from 0.50 ± 0.09 to 0.96 ± 0.04 (Table 2). Statistical analysis revealed two groupings in the data: LNC50, LNC150 and PVAc60% nanoparticles had significantly lower HIC index values ($p<0.05$) compared to the high hydrophobicity nanoparticles, PVAc80% and PS50 (Figure 1b). A full statistical comparison is provided in Supporting Information (Table S1).

Nanoparticle surface hydrophobicity influenced colloidal stability in different dispersion media. All nanoparticle suspensions were stable in water and 5% dextrose at room temperature over four weeks. Microsprayer® aerosolization of 25 µL suspension into 1 mL purified water did not alter the particle size distribution (Figure 2a-e**,** red and green traces). However, differences in colloidal stability were observed when suspensions were aerosolized into a model physiological fluid, i.e. HBSS containing 10% FBS maintained at 37°C. Under those conditions, low hydrophobicity systems (LNC50, LNC150 and PVAc60%) remained stable over 24 h (Figure 2a-c, blue and black traces), while PVAc80% and PS50 aggregated immediately upon exposure to the model physiological fluid (Figure 2d-e, blue traces). At 10 min, the aggregate size was two and six-fold the original particle size for the PVAc80% and PS50 systems respectively, (Figure 2d-e, black traces). By 24 h the aggregates were too large to measure by dynamic light scattering. These observations provide indirect confirmation of the HIC results, as the aggregation of neutral nanoparticles in electrolyte solutions is driven primarily by hydrophobic interactions [45].

3.2 Impact of high surface hydrophobicity nanoparticles on acute respiratory toxicity

Inflammation was measured as neutrophil influx (Figure 3a), hypercellularity (Figure 3b) and cytokine levels (Figures 4a-d) in BAL samples 24h post-exposure to the different nanoformulations. Elevated BAL protein levels were considered indicative of tissue damage and were also measured 24 h nanoparticle post-exposure (Figure 4e). Low hydrophobicity nanoparticle systems (HIC index values < 0.7) showed no evidence of inflammation compared to PVAc80% and PS50 (HIC > 0.8), which both induced an acute dose-dependent inflammatory reaction evidenced through an increase in BAL neutrophils, inflammatory cytokines and, to a lesser extent, total cells counts. The high dose of LNC150 and the low dose of PVAc60% nanoparticles showed mild evidence of tissue damage; however no further trends were observed in the low hydrophobicity nanoparticle group. In contrast, PVAc80% and PS 50 nanoparticle exposure induced a significant dose-dependent increase in BAL protein content, indicative of acute tissue damage.

As reported by others [18, 19, 41], particle size did not appear to influence respiratory toxicity; i.e. the smaller PS50 and LNC50 systems produced findings aligned with particles of similar hydrophobicity rather than size (Figures 3 and 4). The level of PS50 induced inflammation corresponded with that reported in the literature reports for PS beads of similar size and surface area dose [19, 22] (taking into consideration that the total numbers of cells in a mouse lung are roughly one magnitude of order lower than that observed in the rat lung [46]). At the low surface area dose (22 cm^2), PVAc80% was the only nanomaterial on the panel to elicit an inflammatory response in the form of significantly elevated IL-1β, IL-6 and TNF-α levels (Figure 4a-d). At the high surface area dose (220 cm^2) PVAc80% nanoparticles elicited significant release of CXCL1, IL-1β, IL-6 and TNF-α, with PS50 nanoparticles producing statistically equivalent responses in all cytokines apart from TNF-α.

Total protein levels in BAL can be used as a marker of tissue damage [22]. A significant dose-dependent increase in BAL protein levels was observed following treatment with hydrophobic nanomaterials, PVAc80% and PS50 (Figure 4e). LNC150 treatment at the higher dose was also associated with significantly elevated protein levels, indicating potential tissue damage or irritation following exposure to these systems. However, a clear mechanism for this observation is not obvious from the current data set. For example, if the elevated BAL protein levels resulted from a higher exposure level to LNC components, such as the stabilizing surfactant, Solutol® HS15, it would be expected that the high dose LNC50 treatment groups would show a similar effect, which was not the case. Therefore, this observation requires further investigation.

Lung tissue histopathology, a major component of nonclinical safety studies for inhaled pharmaceuticals, was performed in a blinded analysis by an independent pathologist to assess toxicity in response to nanoparticle exposure. Histopathology findings (Figure 5) were broadly concordant with the results of the BAL analysis (Figures 3 and 4). Animals treated with high surface hydrophobicity nanomaterials (Figure 5e-g) showed an elevated incidence of adverse effects, with PVAc80% treatment eliciting a more profound response compared to PS50 according to the pathology report (Figure 5g). Notable findings in response to PVAc60%,

PVAc80% and PS50 nanoparticles included evidence of mild perivascular oedema and bronchiolar epithelial vacuolation in response to nanoparticle exposure (Figure 5g). Both LNC formulations were associated with a lower frequency and severity histopathology findings (Figure 5b,c, g), although the high dose LNC150 treatment was associated with reports of acute bronchopneumonia in three out of five animals. This observation may be related to the significant increase in BAL protein levels observed in this treatment group, although as stated previously further studies are required to understand the underlying mechanism. Increased numbers of alveolar luminal macrophages were observed after administration of all nanoparticle types, although not to levels greater than the vehicle controls (vehicle control images provided in Figure S1, Supporting Information). The cause of this elevation in luminal macrophage numbers is not currently understood, although qualitative assessment of histology data from animals treated with 5% m/v dextrose and 0.9% saline vehicles indicate that the dextrose vehicle may be slightly more irritating to the lung (e.g. causing mild bronchial epithelial hyperplasia, mild thickening of the alveolar walls and mild increases in alveolar macrophage numbers). This hypothesis is currently under investigation in greater detail. It should be noted that the dextrose vehicle was necessary in this study to avoid aggregation of high hydrophobicity nanomaterials prior to administration.

3.3 Macrophage responses to polymeric nanoparticles.

Analysis of the BAL macrophage population revealed two distinct morphological phenotypes following treatment with polymeric nanoparticles. Firstly, a minority population of enlarged macrophages with a finely vacuolated cytoplasm was observed, the frequency of which was dose-dependent in the PVAc80% and PS 50 treatment groups (Figure 6a,b). The second phenotype consisted of macrophages with a coarsely vacuolated cytoplasm (Figure 6a). This phenotype was observed most frequently following treatment with PVAc60% > PVAc80% > PS 50 (Figure 6c).

Preliminary *in vitro* studies performed with PVAc60% and PVAc80% nanoparticles indicated that PVAc60% treatment induced the same coarsely vacuolated phenotype in the J774 cell murine macrophage line (Figure 7c-e) and that this response was dose-dependent. In contrast, PVAc80% exposure to J774 cells did not induce the coarsely vacuolated phenotype under the conditions tested (Figure 7f-h); however the PVAc80% nanoparticles were observed to aggregate substantially in cell culture medium, thus perhaps altering their presentation to cells under *in vitro* conditions. It may be speculated that PVAc60% nanoparticle-related effects occur in response to internalized and processed nanomaterials, while PVAc80% effects may be driven either by small amounts of internalized particles or by responses to external nanoparticle agglomerates. A significant increase in the frequency of apoptotic cells in the total cell population was observed at the highest dose tested (10mg/mL) for both PVAc60% and PVAc80%, whereby PVAc80% exposure led to a significantly higher prevalence of apoptotic cells compared to PVAc60% ($p=0.03$). The MTT assay and MitoView™688 staining indicated that there was no dose-dependent reduction in mitochondrial activity for either nanoparticle type, even at the highest concentrations tested (supplementary data, Figure S2).

4. Discussion

The nanomaterials investigated in this study were carefully chosen to exhibit a spectrum of hydrophobicity values across a range of different material classes. The LNCs were ideal representatives of nanomaterials with relatively hydrophilic surfaces because they are highly stable colloids under physiological conditions and there is little evidence that the pegylated surface is displaced or altered substantially by the presence of biomolecules in physiological fluids [47]. The PVAc nanomaterials are equally useful with respect to studying nanoparticle hydrophobicity, as the core PVAc polymer can be easily modified via controlled hydrolysis generate polymeric NP with a range of hydrophobicity values. Therefore, even if the PVA stabilizer is displaced from the particle surface over the duration of the experiment, the substantial differences in the hydrophobicity values of the core polymers will ensure that the effects of hydrophobicity can still be examined in a valid manner. The observations that the more hydrophilic PVAC60% nanoconstructs showed a greater similarity to the pegylated LNC in terms of colloidal stability and inflammatory profile provide supporting evidence for validity of this approach.

It was hypothesized that increases in nanoparticle surface hydrophobicity would correlate with a higher frequency and severity of adverse pulmonary effects, such as acute inflammation and tissue damage. This hypothesis was based on reports that show high material hydrophobicity to be implicated in the inflammatory foreign body response to implantable medical devices [48-50] as well as studies which demonstrate that hydrophobicity is generally recognized by the immune system as a damage-associated molecular pattern [51, 52]. In order to systematically assess the impact of nanoparticle surface hydrophobicity on pulmonary biocompatibility, a versatile and accessible quantitative method for surface hydrophobicity analysis was required. The HIC method [29] provided the combined advantages of sensitivity, robustness, versatility and accessibility for routine evaluation of nanoparticle surface hydrophobicity. To improve the discriminatory power of the original HIC assay, nanoparticle systems were eluted through three different HIC columns with varying column chemistries and Equation 2 was developed to calculate the HIC index values reported here. This approach is simple, sensitive and can be applied to biomaterials of very different compositions.

Administration of the five nanoparticle systems at two doses revealed that the two nanomaterials with the highest HIC index values (> 0.8) induced significant, dose-dependent inflammatory responses and tissue damage, while nanoparticles with lower HIC index values (~0.5-0.7) were not inflammatory under the conditions tested. The relationship between surface hydrophobicity and respiratory toxicity was not a linear correlation. For example, plots (not shown) of the HIC index value vs. number of neutrophils in BAL reveal low coefficient of determination values: R^2=0.1455 at the 22 cm^2 dose and R^2=0.2901 at the 220 cm^2 dose. Instead, significant inflammation and tissue damage occurred only in high hydrophobicity nanoparticle treatment groups (Figures 3-5).

The relationship between hydrophobicity and toxicity is multifactorial. It is well known that proteins and opsonins may absorb more favorably onto a hydrophobic surface, promoting recognition by phagocytic cells and differences in intracellular processing [53, 54]. In the lung, this role may be filled by surfactant-associated proteins (SP), in particular SP-A, which has been

implicated in recognition and uptake of nanoparticles by alveolar macrophages [53, 55]. In addition, colloidal instability and particle aggregation in the lung lining fluid may be highly influential in promoting an inflammatory response or tissue damage. For example, studies have shown that biopolymer particles larger than 500 nm exhibit preferential uptake by phagocytic cells and elicit a stronger inflammatory response compared to nanoparticles < 500 nm [56]. Furthermore, it would appear that the clustering of nanoparticles during aggregation creates a new entity with an irregular surface that may present a higher pro-inflammatory potential than comparable smooth-surface particles [57]. The *in situ* formation of nanoaggregate structures in lung lining may occur for high surface hydrophobicity particles and it therefore follows that the morphology and stability of such constructs might explain, either entirely or in part, the toxicity profiles observed for PVAc80% and PS50 particles. Finally, it should be noted that the role of mechanical properties, such as particle rigidity / elasticity, has yet to be explored systematically in relation to nanoparticle biocompatibility. Banquay et al [58] have shown that polyacrylamide hydrogel nanoparticles with increasing rigidity achieved through increasing crosslinker density were internalized by macrophage cells in greater amounts compared to low rigidity nanoparticles of the same material. Further, the mechanism of internalization was different, with high rigidity nanoparticles being taken up through clathrin-mediated endocytosis, whereas low rigidity materials were primarily taken up passively through macropinocytosis. It is possible that the low hydrophobicity nanomaterials included in this study (e.g. LNC50, LNC150 and PVAc60%) also have a lower rigidity, which might, in addition to the low hydrophobicity, contribute to their enhancedbiocompatibility profile. Therefore, this parameter requires further study.

The macrophage responses (i.e. elevated numbers of finely and coarsely vacuolated macrophages) to polymeric nanoparticles did not appear to be linked to HIC index or pro-inflammatory potential. Our preliminary investigations with the J774 cell line indicate that the finely vacuolated phenotype may be associated with apoptosis, since J774 cells with this appearance also showed caspase 3/7 activity (Figure 7). The coarsely vacuolated macrophage phenotype has been previously reported following exposure to a wide range of materials, including high molecular weight polymers such as polyethylene glycols [59], poorly soluble pharmaceuticals [60], insoluble nanomaterials such as carbon nanotubes, gold, zinc oxide, titanium dioxide, fullerenes, quantum dots and silica [61, 62], and biomaterial nanoparticles such as non-inflammatory solid lipid nanoparticles [21, 63]. It may be indicative of autophagy, a process which has been increasingly associated with nanoparticle exposure [61, 64]. Autophagy can be triggered by nanoparticle-induced dysfunction or dysregulation of endo-lysosomal pathways, resulting in the formation of large, double-membrane autophagic vacuoles containing cellular debris, such as engulfed material and internal organelles. Evidence suggests that autophagy may not necessarily be a direct pathway leading to cell death, but rather constitutes an adaptive response to stress [65], although the impact of autophagy on long term respiratory health remains to be investigated.

5. Conclusions

Five nanoparticle systems representative of inhaled drug delivery nanoparticles (LNC),

consumer products (PVAc), and experimental model particles (PVAc and PS) were used to explore whether particle surface hydrophobicity could be quantified and correlated with acute respiratory toxicity after pulmonary administration. The results demonstrated that HIC analysis is a versatile, simple quantitative technique that is suitable for routine profiling of nanoparticle surface hydrophobicity. Further, the HIC index provides a scale to facilitate comparison of nanoparticles spanning different material classes, making it useful for quantitative-structure-activity relationships in biocompatibility studies.

It was demonstrated that high hydrophobicity nanomaterials (HIC index >0.8) induced significant acute respiratory toxicity following a single-dose administration, while nanoparticles with low/intermediate hydrophobicity (HIC index <0.7) elicited little to no inflammatory response or tissue damage. Indeed, the most hydrophilic nanomaterial in this study, LNC50, demonstrated a high biocompatibility making this a promising nanoformulation to take forward into nonclinical safety studies. In conclusion, the HIC index value offers a versatile and accessible method for the quantification of nanoparticle surface hydrophobicity, which may be useful in the design of safe nanomedicines for inhalation therapy.

Acknowledgements

The authors would like to thank the UK Medical Research Council for funding this study (G0900953).

Author Contributions

The study was designed by S. Jones, B. Forbes, D. Spina, C. Page and L. A. Dailey. Nanoparticle manufacture, optimization, and characterization was performed by M.C. Jones, A. Morgan and A. Patel. Animal studies were conducted by Y. Riffo-Vasquez, D. Spina and M.C. Jones. Cell culture experiments were performed by E. Hoffman. All authors contributed to writing and evaluation of the manuscript.

References

[1] B. Bharatwaj, L.B. Wu, J.A. Whittum-Hudson, S.R.P. da Rocha, The potential for the noninvasive delivery of polymeric nanocarriers using propellant-based inhalers in the treatment of Chlamydial respiratory infections, Biomaterials, 31 (2010) 7376-7385.

[2] S. Weber, A. Zimmer, J. Pardeike, Solid Lipid Nanoparticles (SLN) and Nanostructured Lipid Carriers (NLC) for pulmonary application: A review of the state of the art, Eur. J. Pharm. Biopharm.

[3] O. Taratula, A. Kuzmov, M. Shah, O.B. Garbuzenko, T. Minko, Nanostructured lipid carriers as multifunctional nanomedicine platform for pulmonary co-delivery of anticancer drugs and siRNA, J. Controlled Rel., 171 (2013) 349-357.

[4] R. Pandey, A. Sharma, A. Zahoor, S. Sharma, G. Khuller, B. Prasad, Poly (DL-lactide-co-glycolide) nanoparticle-based inhalable sustained drug delivery system for experimental tuberculosis, J. Antimicrob. Chemother., 52 (2003) 981-986.

[5] E. Rytting, J. Nguyen, X. Wang, T. Kissel, Biodegradable polymeric nanocarriers for pulmonary drug delivery, Expert Opin. Drug. Deliv., 5 (2008) 629-639.

[6] M. Beck-Broichsitter, O.M. Merkel, T. Kissel, Controlled pulmonary drug and gene delivery using polymeric nano-carriers, J. Controlled Rel., 161 (2012) 214-224.

[7] M.M. Bailey, C.J. Berkland, Nanoparticle formulations in pulmonary drug delivery, Med. Res. Rev., 29 (2009) 196-212.

[8] A. Nel, T. Xia, L. Mädler, N. Li, Toxic Potential of Materials at the Nanolevel, Science, 311 (2006) 622-627.

[9] K. Donaldson, L. Tran, L. Jimenez, R. Duffin, D. Newby, N. Mills, W. MacNee, V. Stone, Combustion-derived nanoparticles: A review of their toxicology following inhalation exposure, Particle and Fibre Toxicology, 2 (2005) 10.

[10] S. Bakand, A. Hayes, F. Dechsakulthorn, Nanoparticles: a review of particle toxicology following inhalation exposure, Inhalation Toxicology, 24 (2012) 125-135.

[11] Y. Tang, S. Han, H. Liu, X. Chen, L. Huang, X. Li, J. Zhang, The role of surface chemistry in determining in vivo biodistribution and toxicity of CdSe/ZnS core–shell quantum dots, Biomaterials, 34 (2013) 8741-8755.

[12] K. Luyts, D. Napierska, B. Nemery, P.H.M. Hoet, How physico-chemical characteristics of nanoparticles cause their toxicity: complex and unresolved interrelations, Environ Sci-Proc Imp, 15 (2013) 23-38.

[13] H.Y. Zhang, Z.X. Ji, T. Xia, H. Meng, C. Low-Kam, R. Liu, S. Pokhrel, S.J. Lin, X. Wang, Y.P. Liao, M.Y. Wang, L.J. Li, R. Rallo, R. Damoiseaux, D. Telesca, L. Madler, Y. Cohen, J.I. Zink, A.E. Nel, Use of Metal Oxide Nanoparticle Band Gap To Develop a Predictive Paradigm for Oxidative Stress and Acute Pulmonary Inflammation, Acs Nano, 6 (2012) 4349-4368.

[14] W.S. Cho, R. Duffin, F. Thielbeer, M. Bradley, I.L. Megson, W. MacNee, C.A. Poland, C.L. Tran, K. Donaldson, Zeta Potential and Solubility to Toxic Ions as Mechanisms of Lung Inflammation Caused by Metal/Metal Oxide Nanoparticles, Toxicological Sciences, 126 (2012) 469-477.

[15] A. Beyerle, A. Braun, O. Merkel, F. Koch, T. Kissel, T. Stoeger, Comparative in vivo study of poly(ethylene imine)/siRNA complexes for pulmonary delivery in mice, Journal of Controlled Release, 151 (2011) 51-56.

[16] S.J. Kemp, A.J. Thorley, J. Gorelik, M.J. Seckl, M.J. O'Hare, A. Arcaro, Y. Korchev, P. Goldstraw, T.D. Tetley, Immortalization of Human Alveolar Epithelial Cells to Investigate Nanoparticle Uptake, American Journal of Respiratory Cell and Molecular Biology, 39 (2008) 591-597.

[17] Poland CA, Duffin R, Donaldson K: High Aspect Ratio Nanoparticles and the Fibre Pathogenicity Paradigm. In Nanotoxicity: in vivo and in vitro models to health risks. Edited by Sahu SC and Casciano D. Chichester:John Wiley and Sons; 2009:61-80.

[18] D.M. Brown, M.R. Wilson, W. MacNee, V. Stone, K. Donaldson, Size-dependent proinflammatory effects of ultrafine polystyrene particles: A role for surface area and oxidative stress in the enhanced activity of ultrafines, Toxicology and Applied Pharmacology, 175 (2001) 191-199.

[19] R. Duffin, L. Tran, D. Brown, V. Stone, K. Donaldson, Proinflammogenic effects of low-toxicity and metal nanoparticles in vivo and in vitro: Highlighting the role of particle surface area and surface reactivity, Inhalation Toxicology, 19 (2007) 849-856.

[20] A.D. Maynard, D.B. Warheit, M.A. Philbert, The new toxicology of sophisticated materials: nanotoxicology and beyond, Toxicol Sci, 120 Suppl 1 (2011) S109-129.

[21] M. Nassimi, C. Schleh, H.-D. Lauenstein, R. Hussein, K. Lübbers, G. Pohlmann, S. Switalla, K. Sewald, M. Müller, N. Krug, C.C. Müller-Goymann, A. Braun, Low cytotoxicity of solid lipid nanoparticles in in vitro and ex vivo lung models, Inhalation Toxicology, 21 (2009) 104-109.

[22] L.A. Dailey, N. Jekel, L. Fink, T. Gessler, T. Schmehl, M. Wittmar, T. Kissel, W. Seeger, Investigation of the proinflammatory potential of biodegradable nanoparticle drug delivery systems in the lung, Toxicology and Applied Pharmacology, 215 (2006) 100-108.

[23] A. Beyerle, A. Braun, A. Banerjee, N. Ercal, O. Eickelberg, T.H. Kissel, T. Stoeger, Inflammatory responses to pulmonary application of PEI-based siRNA nanocarriers in mice, Biomaterials, 32 (2011) 8694-8701.

[24] X.R. Xia, N.A. Monteiro-Riviere, S. Mathur, X.F. Song, L.S. Xiao, S.J. Oldenberg, B. Fadeel, J.E. Riviere, Mapping the Surface Adsorption Forces of Nanomaterials in Biological Systems, Acs Nano, 5 (2011) 9074-9081.

[25] X.R. Xia, N.A. Monteiro-Riviere, J.E. Riviere, An index for characterization of nanomaterials in biological systems, Nat Nanotechnol, 5 (2010) 671-675.

[26] L.A. Dailey, T. Schmehl, T. Gessler, M. Wittmar, F. Grimminger, W. Seeger, T. Kissel, Nebulization of biodegradable nanoparticles: impact of nebulizer technology and nanoparticle characteristics on aerosol features, Journal of Controlled Release, 86 (2003) 131-144.

[27] Y. Xiao, M.R. Wiesner, Characterization of surface hydrophobicity of engineered nanoparticles, J Hazard Mater, 215 (2012) 146-151.

[28] S. Doktorovova, R. Shegokar, P. Martins-Lopes, A.M. Silva, C.M. Lopes, R.H. Muller, E.B. Souto, Modified Rose Bengal assay for surface hydrophobicity evaluation of cationic solid lipid nanoparticles (cSLN), European Journal of Pharmaceutical Sciences, 45 (2012) 606-612.

[29] H. Carstensen, B.W. Muller, R.H. Muller, Adsorption of Ethoxylated Surfactants on Nanoparticles .1. Characterization by Hydrophobic Interaction Chromatography, International Journal of Pharmaceutics, 67 (1991) 29-37.

[30] M.O. Gul, S.A. Jones, L.A. Dailey, H. Nacer, Y.M. Ma, F. Sadouki, R. Hider, A. Ararnan, B. Forbes, A poly(vinyl alcohol) nanoparticle platform for kinetic studies of

inhaled particles, Inhalation Toxicology, 21 (2009) 631-640.

[31] American College of Toxicology: Final Report on the Safety Assessment of Polyvinyl Acetate, Int J Toxicol 1992,11: 465-473.

[32] A. Cahouet, B. Denizot, F. Hindre, C. Passirani, B. Heurtault, M. Moreau, J.J. Le Jeune, J.P. Benoit, Biodistribution of dual radiolabeled lipidic nanocapsules in the rat using scintigraphy and gamma counting, International Journal of Pharmaceutics, 242 (2002) 367-371.

[33] A.B. Dhanikula, N.M. Khalid, S.D. Lee, R. Yeung, V. Risovic, K.M. Wasan, J.C. Leroux, Long circulating lipid nanocapsules for drug detoxification, Biomaterials, 28 (2007) 1248-1257.

[34] F. Lacoeuille, E. Garcion, J.P. Benoit, A. Lamprecht, Lipid nanocapsules for intracelluar drug delivery of anticancer drugs, J Nanosci Nanotechno, 7 (2007) 4612-4617.

[35] E. Garcion, A. Lamprecht, B. Heurtault, A. Paillard, A. Aubert-Pouessel, B. Denizot, P. Menei, J.P. Benoit, A new generation of anticancer, drug-loaded, colloidal vectors reverses multidrug resistance in glioma and reduces tumor progression in rats, Molecular Cancer Therapeutics, 5 (2006) 1710-1722.

[36] J. Hureaux, F. Lagarce, F. Gagnadoux, L. Vecellio, A. Clavreul, E. Roger, M. Kempf, J.L. Racineux, P. Diot, J.P. Benoit, T. Urban, Lipid nanocapsules: Ready-to-use nanovectors for the aerosol delivery of paclitaxel, European Journal of Pharmaceutics and Biopharmaceutics, 73 (2009) 239-246.

[37] J. Chana, B. Forbes, S.A. Jones, The Synthesis of High Molecular Weight Partially Hydrolysed Poly(vinyl alcohol) Grades Suitable for Nanoparticle Fabrication, J Nanosci Nanotechno, 8 (2008) 5739-5747.

[38] S.K. Sahoo, J. Panyam, S. Prabha, V. Labhasetwar, Residual polyvinyl alcohol associated with poly (D,L-lactide-co-glycolide) nanoparticles affects their physical properties and cellular uptake, Journal of Controlled Release, 82 (2002) 105-114.

[39] B. Heurtault, P. Saulnier, B. Pech, J.P. Benoit, J.E. Proust, Interfacial stability of lipid nanocapsules, Colloid Surface B, 30 (2003) 225-235.

[40] A. Nag, G. Mitra, P.C. Ghosh, A colorimetric assay for estimation of polyethylene glycol and polyethylene glycolated protein using ammonium ferrothiocyanate, Anal Biochem, 237 (1996) 224-231.

[41] T.M. Sager, V. Castranova, Surface area of particle administered versus mass in determining the pulmonary toxicity of ultrafine and fine carbon black: comparison to ultrafine titanium dioxide, Particle and Fibre Toxicology, 6 (2009).

[42] M. Bivas-Benita, R. Zwier, H.E. Junginger, G. Borchard, Non-invasive pulmonary aerosol delivery in mice by the endotracheal route, European Journal of Pharmaceutics and Biopharmaceutics, 61 (2005) 214-218.

[43] Draft OECD Guidance Document on Histopathology for inhalation toxicity studies,

Supporting TG 412 (Subacute Inhalation Toxicity: 28-Day) and TG 413 (Subchronic Inhalation Toxicity: 90-Day) http://www.oecd.org/chemicalsafety/testing/43822718.pdf (accessed 20 February 2011).

[44] A. Grenha, C.I. Grainger, L.A. Dailey, B. Seijo, G.P. Martin, C. Remunan-Lopez, B. Forbes, Chitosan nanoparticles are compatible with respiratory epithelial cells in vitro, European Journal of Pharmaceutical Sciences, 31 (2007) 73-84.

[45] A.E. Nel, L. Madler, D. Velegol, T. Xia, E.M.V. Hoek, P. Somasundaran, F. Klaessig, V. Castranova, M. Thompson, Understanding biophysicochemical interactions at the nano-bio interface, Nat Mater, 8 (2009) 543-557.

[46] E. Bermudez, J.B. Mangum, B.A. Wong, B. Asgharian, P.M. Hext, D.B. Warheit, J.I. Everitt, Pulmonary responses of mice, rats, and hamsters to subchronic inhalation of ultrafine titanium dioxide particles, Toxicological Sciences, 77 (2004) 347-357.

[47] A. Vonarbourg, C. Passirani, P. Saulnier, P. Simard, J.C. Leroux, J.P. Benoit, Evaluation of pegylated lipid nanocapsules versus complement system activation and macrophage uptake, J Biomed Mater Res A, 78A (2006) 620-628.

[48] D.T. Chang, J.A. Jones, H. Meyerson, E. Colton, I.K. Kwon, T. Matsuda, J.M. Anderson, Lymphocyte/macrophage interactions: Biomaterial surface-dependent cytokine, chemokine, and matrix protein production, J Biomed Mater Res A, 87A (2008) 676-687.

[49] J.A. Jones, D.T. Chang, H. Meyerson, E. Colton, I.K. Kwon, T. Matsuda, J.M. Anderson, Proteomic analysis and quantification of cytokines and chemokines from biomaterial surface-adherent macrophages and foreign body giant cells, J Biomed Mater Res A, 83A (2007) 585-596.

[50] P. Thevenot, W.J. Hu, L.P. Tang, Surface chemistry influences implant biocompatibility, Curr Top Med Chem, 8 (2008) 270-280.

[51] D.F. Moyano, M. Goldsmith, D.J. Solfiell, D. Landesman-Milo, O.R. Miranda, D. Peer, V.M. Rotello, Nanoparticle Hydrophobicity Dictates Immune Response, Journal of the American Chemical Society, 134 (2012) 3965-3967.

[52] S.Y. Seong, P. Matzinger, Hydrophobicity: an ancient damage-associated molecular pattern that initiates innate immune responses, Nat Rev Immunol, 4 (2004) 469-478.

[53] C.A. Ruge, U.F. Schaefer, J. Herrmann, J. Kirch, O. Canadas, M. Echaide, J. Perez-Gil, C. Casals, R. Muller, C.M. Lehr, The Interplay of Lung Surfactant Proteins and Lipids Assimilates the Macrophage Clearance of Nanoparticles, Plos One, 7 (2012).

[54] R. Singh, J.W. Lillard, Nanoparticle-based targeted drug delivery, Exp Mol Pathol, 86 (2009) 215-223.

[55] C.A. Ruge, J. Kirch, O. Canadas, M. Schneider, J. Perez-Gil, U.F. Schaefer, C. Casals, C.M. Lehr, Uptake of nanoparticles by alveolar macrophages is triggered by surfactant protein A, Nanomed-Nanotechnol, 7 (2011) 690-693.

[56] R. Nicolete, D.F. dos Santos, L.H. Faccioli, The uptake of PLGA micro or nanoparticles by

macrophages provokes distinct in vitro inflammatory response, Int Immunopharmacol, 11 (2011) 1557-1563.

[57] C.A. Vaine, M.K. Patel, J.T. Zhu, E. Lee, R.W. Finberg, R.C. Hayward, E.A. Kurt-Jones, Tuning Innate Immune Activation by Surface Texturing of Polymer Microparticles: The Role of Shape in Inflammasome Activation, Journal of Immunology, 190 (2013) 3525-3532.

[58] X. Banquy, F. Suarez, A. Argaw, J.M. Rabanel, P. Grutter, J.F. Bouchard, P. Hildgen, S. Giasson, Effect of mechanical properties of hydrogel nanoparticles on macrophage cell uptake, Soft Matter, 5 (2009) 3984-3991.

[59] D.G. Rudmann, J.T. Alston, J.C. Hanson, S. Heidel, High Molecular Weight Polyethylene Glycol Cellular Distribution and PEG-associated Cytoplasmic Vacuolation Is Molecular Weight Dependent and Does Not Require Conjugation to Proteins, Toxicologic pathology, 41 (2013) 970-983.

[60] K.J. Nikula, J.E. McCartney, T. McGovern, G.K. Miller, M. Odin, M.V. Pino, M.D. Reed, (2013) STP Position Paper: Interpreting the Significance of Increased Alveolar Macrophages in Rodents following Inhalation of Pharmaceutical Materials, Toxicol. Pathol., in press.

[61] S.T. Stern, P.P. Adiseshaiah, R.M. Crist, Autophagy and lysosomal dysfunction as emerging mechanisms of nanomaterial toxicity, Particle and Fibre Toxicology, 9 (2012).

[62] S.T. Stern, D.N. Johnson, Role for nanomaterial-autophagy interaction in neurodegenerative disease, Autophagy, 4 (2008) 1097-1100.

[63] M. Nassimi, C. Schleh, H.D. Lauenstein, R. Hussein, H.G. Hoymann, W. Koch, G. Pohlmann, N. Krug, K. Sewald, S. Rittinghausen, A. Braun, C. Muller-Goymann, A toxicological evaluation of inhaled solid lipid nanoparticles used as a potential drug delivery system for the lung, European Journal of Pharmaceutics and Biopharmaceutics, 75 (2010) 107-116.

[64] S.T. Stern, B.S. Zolnik, C.B. McLeland, J. Clogston, J.W. Zheng, S.E. McNeil, Induction of autophagy in porcine kidney cells by quantum dots: A common cellular response to nanomaterials?, Toxicological Sciences, 106 (2008) 140-152.

[65] C. Jin, Y. Liu, L. Sun, T. Chen, Y. Zhang, A. Zhao, X. Wang, M. Cristau, K. Wang, W. Jia, Metabolic profiling reveals disorder of carbohydrate metabolism in mouse fibroblast cells induced by titanium dioxide nanoparticles, J Appl Toxicol, (2012).

Table 1. Nanoparticle dose metrics for in vivo studies.

Nanoparticle type	Surface area dose (cm^2 per lung)	Mass dose (μg per lung)	Suspension concentration (mg mL^{-1})
50-nm particles (LNC50, PS50)	22	~20	~0.8
	220	~200	~8
150-nm particles (LNC150, PVAc60%/80%)	22	~50	~2
	220	~500	~20

Table 2. Physicochemical properties of the five nanoparticles used in this study following manufacture. *Values listed represent the mean ± standard deviation of n=3 individual batches.*

Nanoparticle type	Hydrodynamic diameter in water (nm)	PDI	Zeta potential in 6.3 mM NaCl (mV)	Residual stabilizer following purification (mg mL^{-1})
LNC50	43 ± 3	0.10 ± 0.03	-7 ± 4	< 0.5
LNC150	144 ± 3	0.15 ± 0.03	-4 ± 1	< 0.5
PVAc60%	160 ± 8	0.09 ± 0.03	-3 ± 0	< 0.4
PVAc80%	172 ± 11	0.15 ± 0.03	-4 ± 1	< 0.4
PS50	54 ± 3	0.05 ± 0.03	-25 ± 6	Undisclosed

Figure captions

Figure 1. HIC index values of the five nanoparticle systems. *(a) The retention values (%) for each nanoparticle system following elution through butyl-, phenyl- and octyl-modified HIC columns are depicted. Values listed represent the mean ± standard deviation of n=3 individual nanoparticle batches. (b) Calculated HIC index values for three replicate batches of each nanoparticle system. (*) p <0.05.*

Figure 2. Colloidal stability of the five nanoparticle systems. *Representative particle size distribution curves of the three low hydrophobicity nanoparticle systems (HIC index <0.7; a-c) and high hydrophobicity systems (HIC index >0.8; d,e). Particles sizes were measured after particle manufacture in water at 25°C (red traces; a-e) and after aerosolization of a 5% m/v dextrose suspension into an excess of water at 25°C (green traces; a-e). To model nanoparticle stability in physiological fluids, particle sizes were measured after aerosolization of a 5% m/v dextrose suspension into an excess of FBS-supplemented HBSS at 37°C at t= 0 h (blue traces; a-e), t=24h (black traces; a-c) or t=10 min (black traces; d,e). All distribution curves are representative of at least n=3 different nanoparticle batches.*

Figure 3. Neutrophil influx and hypercellularity in the BAL cellular fraction following exposure to nanomaterials with increasing surface hydrophobicity. *Neutrophil count (a) and total cell count (b) in BAL 24 h post-administration of vehicle control, 22 or 220 cm^2 surface area dose of nanoparticles to mice. Values represent the mean ± standard deviation of n=5-12 animals per group. (*) p <0.05, (**) p < 0.01, (***) p<0.001.*

Figure 4. Pro-inflammatory cytokines and total protein content in BAL following exposure to nanomaterials with increasing surface hydrophobicity. *BAL levels of CXCL1(a), IL-1β (b),*

IL-6 (c), TNF-α (d) and total protein content (e) in BAL 24 h post-administration of vehicle control, 22 or 220 cm^2 surface area dose of nanoparticles to mice. Values represent the mean
± standard deviation of n=5-12 animals per group. (*) p <0.05, (**) p < 0.01, (***) p<0.001.

Figure 5. Histopathology of lung tissue exposed to nanomaterials with increasing surface hydrophobicity. *Representative images of a naïve lung (a) compared with lung tissue harvested from mice 24 h after LNC50 (b), LNC150 (c), PVAc60% (d), PVAc80% (e) or PS50(f) treatment at a nanoparticle surface area dose of 220 cm^2 (20x magnification; scale bars =100 μm). (g) Evaluation of the frequency of pulmonary adverse events and severity scores (scale: 0-5) based on a blind assessment of lung histopathology by an independent pathologist, n=5 animals for each nanoparticle type administered.*

Figure 6. Macrophage responses following exposure to nanomaterials with increasing surface hydrophobicity*. (a) Representative images (40x magnification) showing macrophages from untreated animals (left image), enlarged macrophages with a finely vacuolated cytoplasm (center image; taken from an animal in the PVAc80% treatment group) and macrophages with a coarsely vacuolated cytoplasm (right image; taken from an animal in the PVAc60% treatment group). The prevalence of macrophages with finely vacuolated cytoplasm (b) and coarsely vacuolated cytoplasm (c), expressed as a percentage of the total macrophage population 24 h post-treatment with vehicle control, 22, and 220 cm^2 of each nanomaterial. Columns represent the mean ± standard deviation from n=5-12 animals per group. (*) p <0.05, (**) p < 0.01, (***) p<0.001.*

Figure 7. J774 macrophage morphology and frequency of apoptosis in response to PVAc 60% and PVAc80% nanoparticle exposure*. Light transmission and confocal laser scanning micrographs of live J774 cells 24 h post-treatment with (a) cell culture medium (negative control), (b) 0.4 mg mL^{-1} PVA (PVAc nanoparticle vehicle control) or 0.5-10 mg/mL PVAc60% (c-e) and PVAc80% (f-h) nanoparticles. Green fluorescence depicts the presence of caspase 3/7 activity (apoptosis), while the corresponding light transmission images highlight dose-dependent vacuolization in response to PVAc60% exposure (b-d). A semi-quantitative image analysis of the frequency of apoptotic cells (caspase 3/7 positive cells, % of total population) was calculated from analysis of three independent images per samples (i). (*) p <0.05, (**) p < 0.01, (***) p<0.001.*

Figure 1

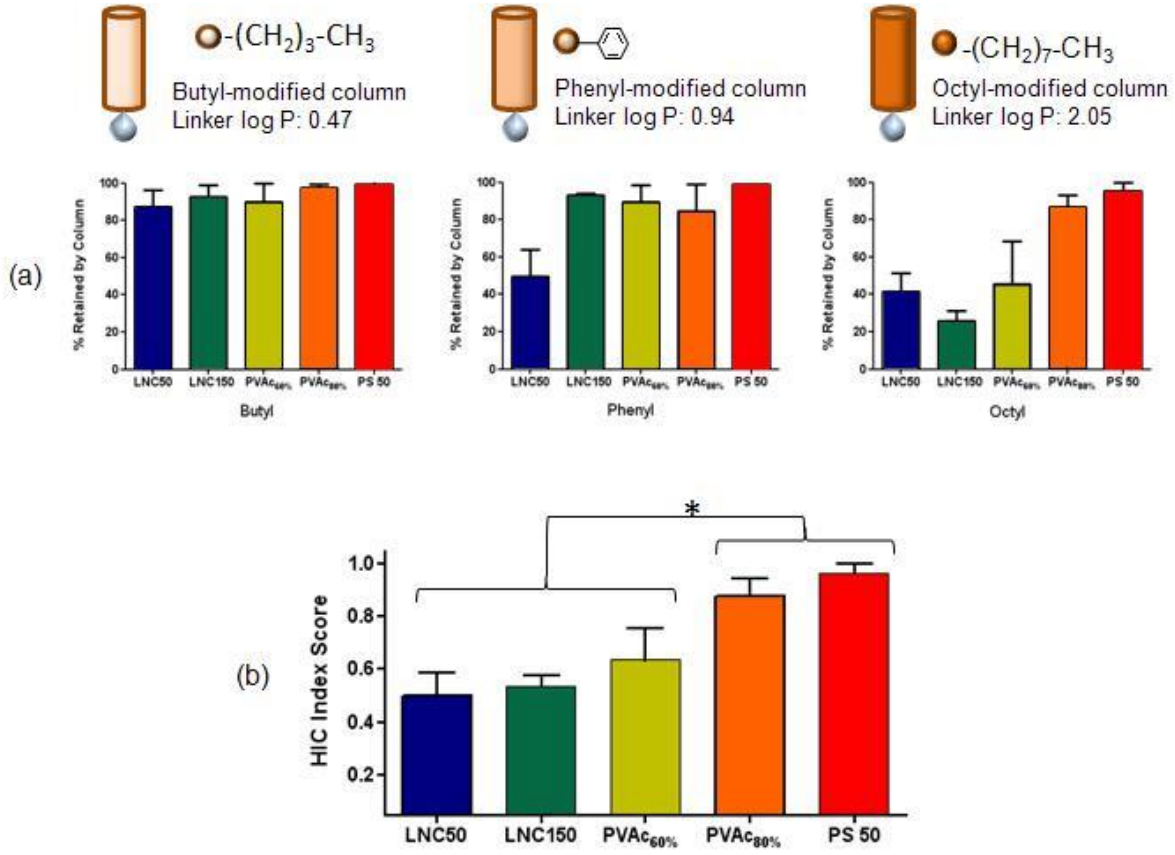
-(CH2)3-CH3
Butyl-modified column
Linker log P: 0.47
Phenyl-modified column
Linker log P: 0.94
-(CH2)7-CH3
Octyl-modified column
Linker log P: 2.05
(a)
% Retained by Column
LNC50
LNC150
PVAc60%
PVAc80%
PS 50
Butyl
Phenyl
Octyl
(b)
HIC Index Score
*

Figure 2

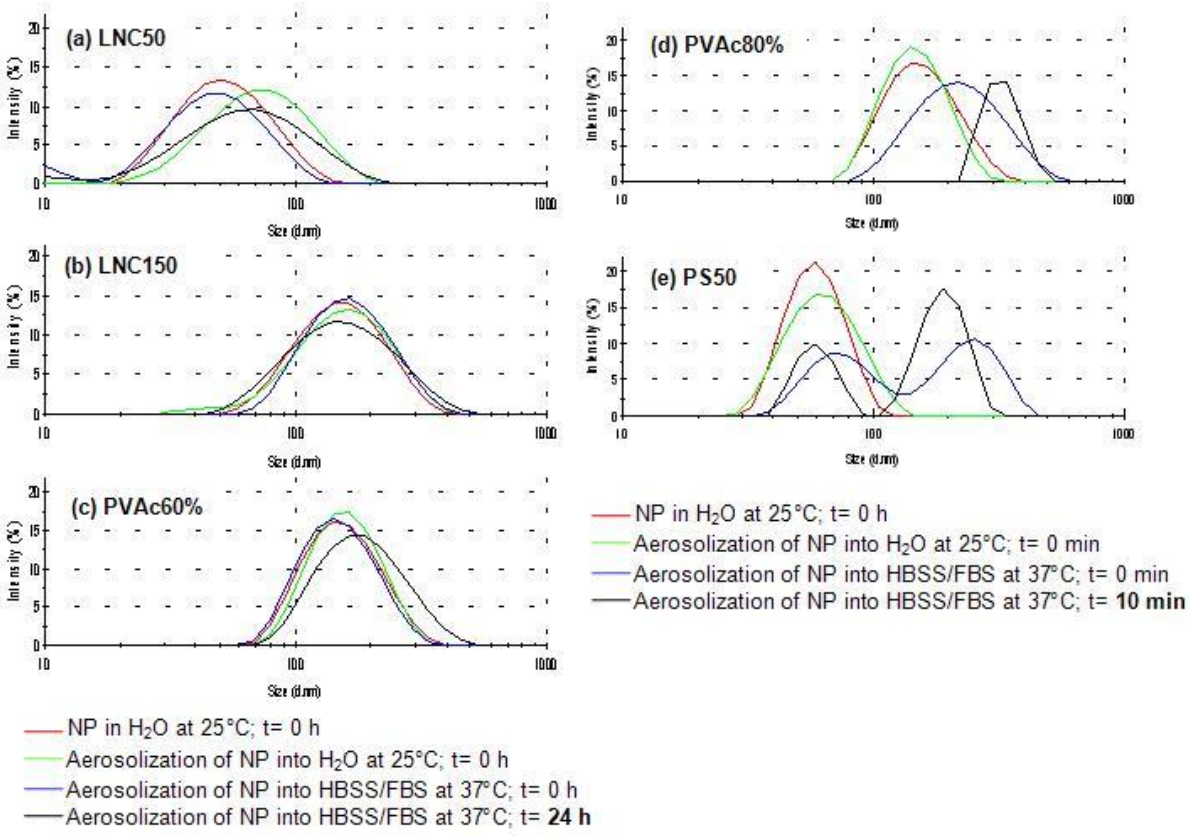
(a) LNC50
(b) LNC150
(c) PVAc60%
(d) PVAc80%
(e) PS50
Intensity (%)
Size (d.nm)
NP in H2O at 25°C; t= 0 h
Aerosolization of NP into H2O at 25°C; t= 0 h
Aerosolization of NP into HBSS/FBS at 37°C; t= 0 h
Aerosolization of NP into HBSS/FBS at 37°C; t= 24 h
NP in H2O at 25°C; t= 0 h
Aerosolization of NP into H2O at 25°C; t= 0 min
Aerosolization of NP into HBSS/FBS at 37°C; t= 0 min
Aerosolization of NP into HBSS/FBS at 37°C; t= 10 min

Figure 3

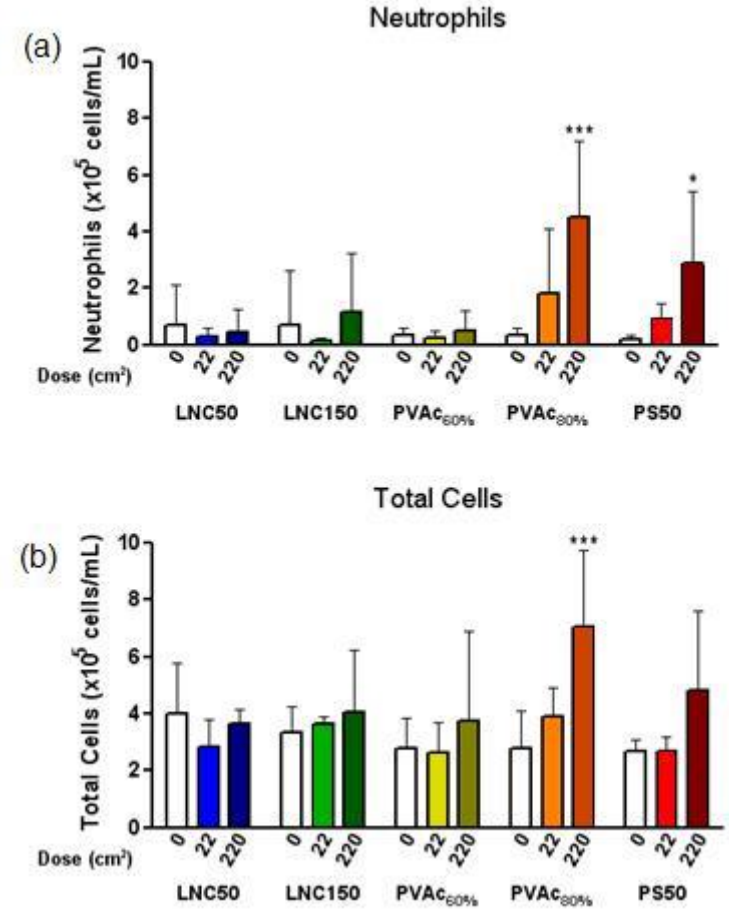
Neutrophils
(a)
Neutrophils (x10^5 cells/mL)
10
8
6
4
2
0
***
*
Dose (cm²)
0
22
220
LNC50
LNC150
PVAc60%
PVAc80%
PS50
Total Cells
(b)
Total Cells (x10^5 cells/mL)
10
8
6
4
2
0
***
Dose (cm²)
0
22
220
LNC50
LNC150
PVAc60%
PVAc80%
PS50

Figure 4

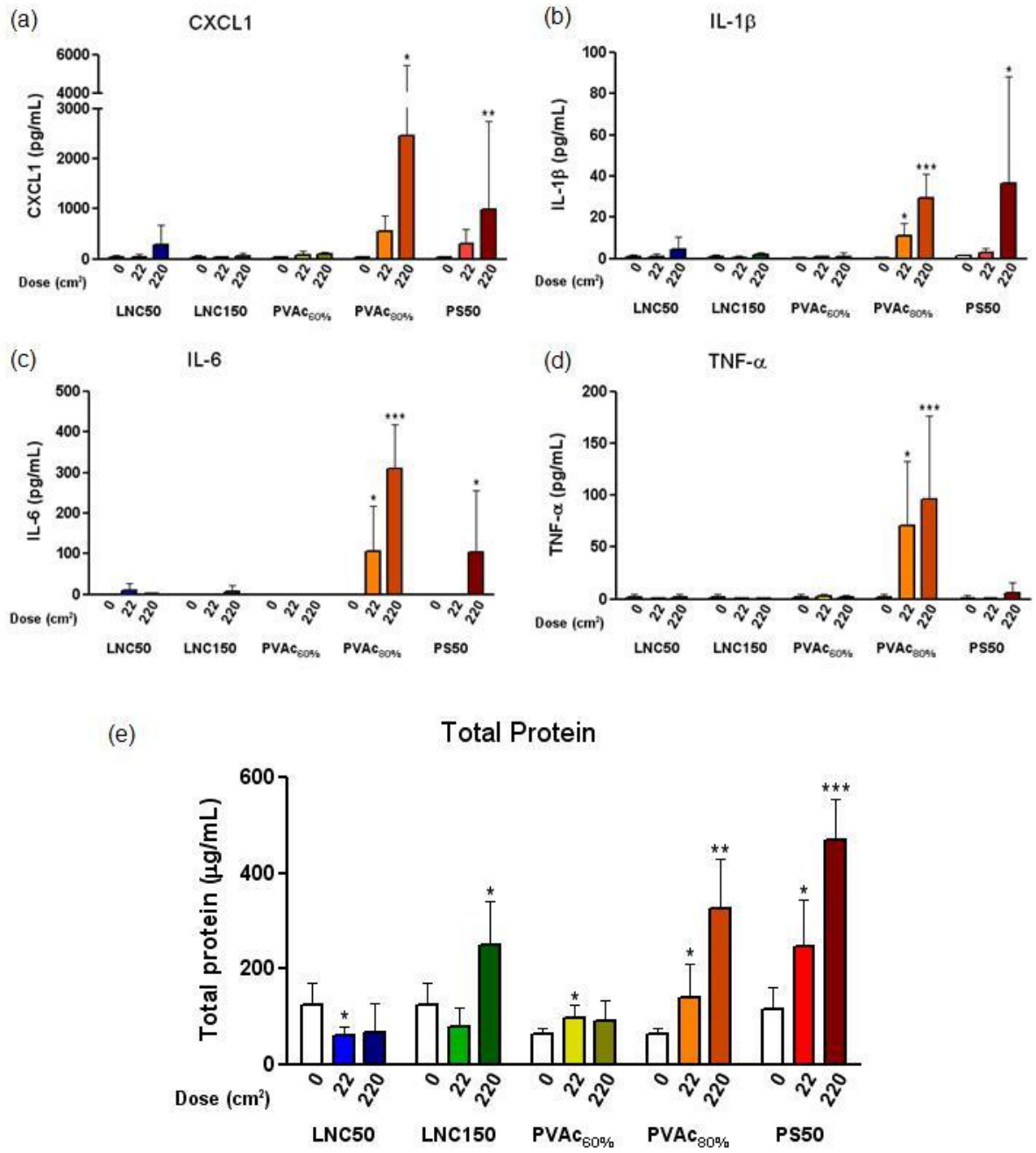
(a)
CXCL1
CXCL1 (pg/mL)
6000
4000
3000
2000
1000
0
Dose (cm²)
0
22
220
LNC50
LNC150
PVAc60%
PVAc80%
PS50
(b)
IL-1β
IL-1β (pg/mL)
100
80
60
40
20
0
(c)
IL-6
IL-6 (pg/mL)
500
400
300
200
100
0
(d)
TNF-α
TNF-α (pg/mL)
200
150
100
50
0
(e)
Total Protein
Total protein (µg/mL)
600
400
200
0

Figure 5

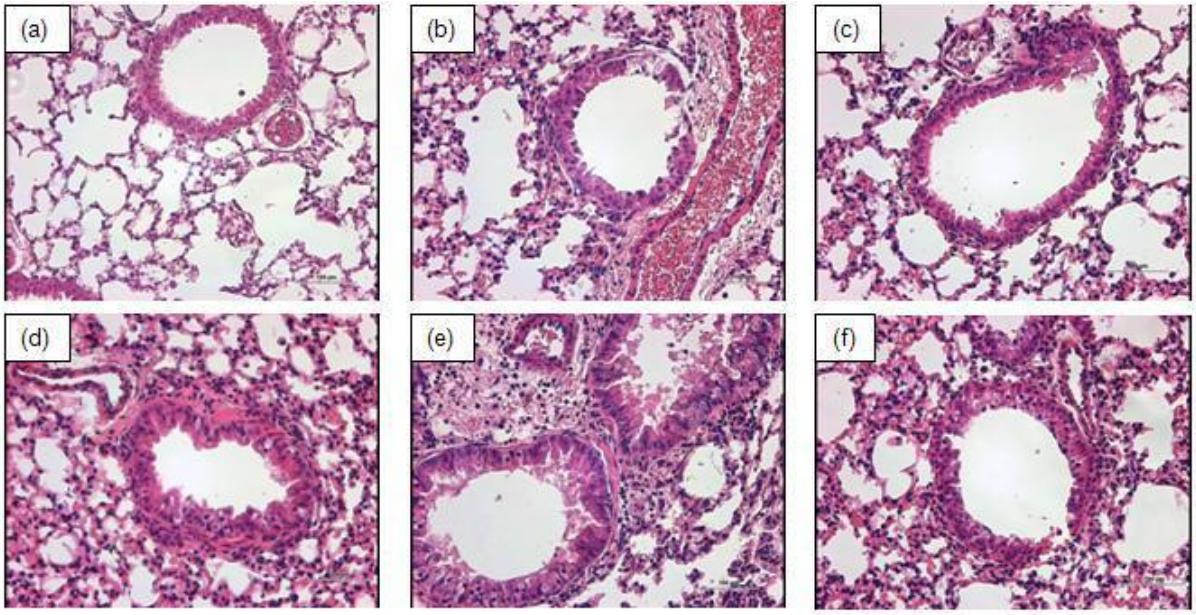

(g) Heat map of adverse events and severity scores based on lung tissue histopathology

Observations	Vehicles			LNC50 (cm^2)		LNC150 (cm^2)		PVAc60% (cm^2)		PVAc80% (cm^2)		PS50 (cm^2)	
	LNC	PVA	PS	22	220	22	220	22	220	22	220	22	220
Bronchiolar epithelial vacuolation	0.0	0.8	0.0	0.0	0.0	0.0	0.0	0.2	0.0	1.2	0.4	1.0	0.0
Acute bronchopneumonia	0.0	0.0	0.0	0.0	0.0	0.0	1.3	0.0	0.0	0.2	1.8	0.0	0.0
Perivascular oedema	0.0	0.0	0.0	0.0	0.0	0.0	0.0	0.4	0.6	0.6	1.0	1.4	0.0
Alveolar luminal macrophages	0.6	1.4	0.8	0.0	0.2	0.4	1.0	1.6	0.6	0.4	0.8	0.2	0.2
Intra alveolar fibrin	0.0	0.0	0.0	0.0	0.0	0.0	0.0	0.0	0.4	0.0	0.0	0.0	0.0
Intra alveolar haemorrhage	0.0	0.0	0.0	0.0	0.0	0.0	0.0	0.0	0.4	0.0	0.4	0.0	0.0

Key
0/5 animals
1/5 animals
2/5 animals
3/5 animals
4/5 animals
5/5 animals

Figure6

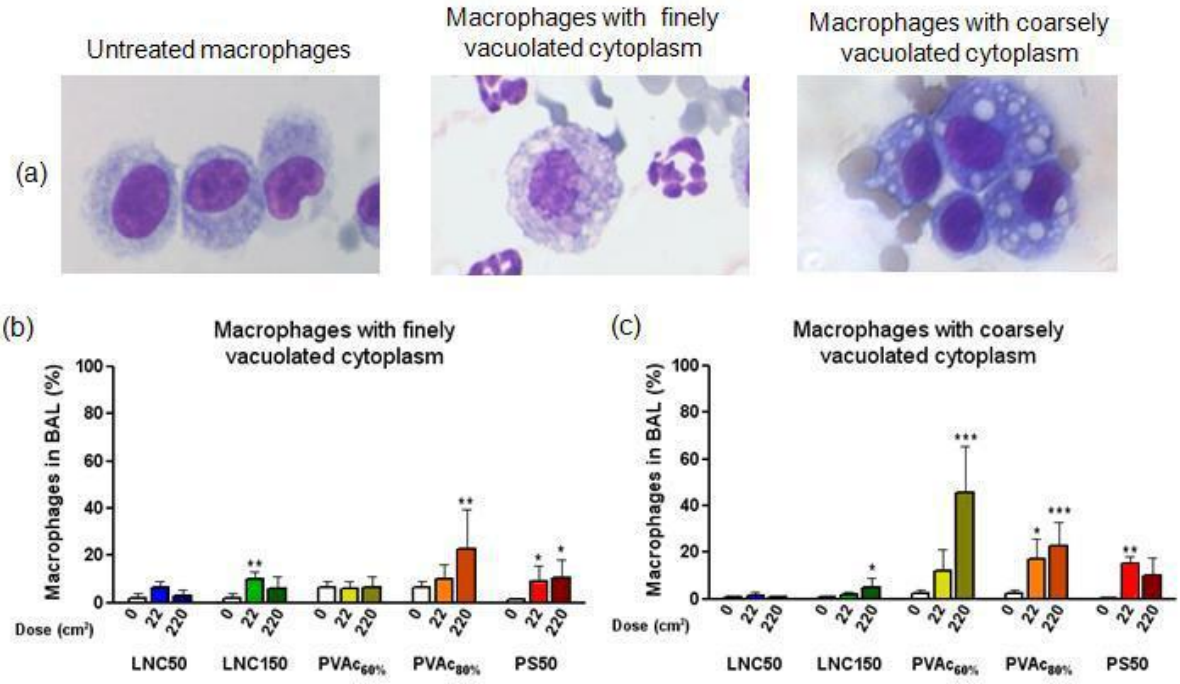
Untreated macrophages
Macrophages with finely vacuolated cytoplasm
Macrophages with coarsely vacuolated cytoplasm
(a)
(b)
Macrophages with finely vacuolated cytoplasm
Macrophages in BAL (%)
Dose (cm²)
LNC50
LNC150
PVAc60%
PVAc80%
PS50
(c)
Macrophages with coarsely vacuolated cytoplasm

Figure 7

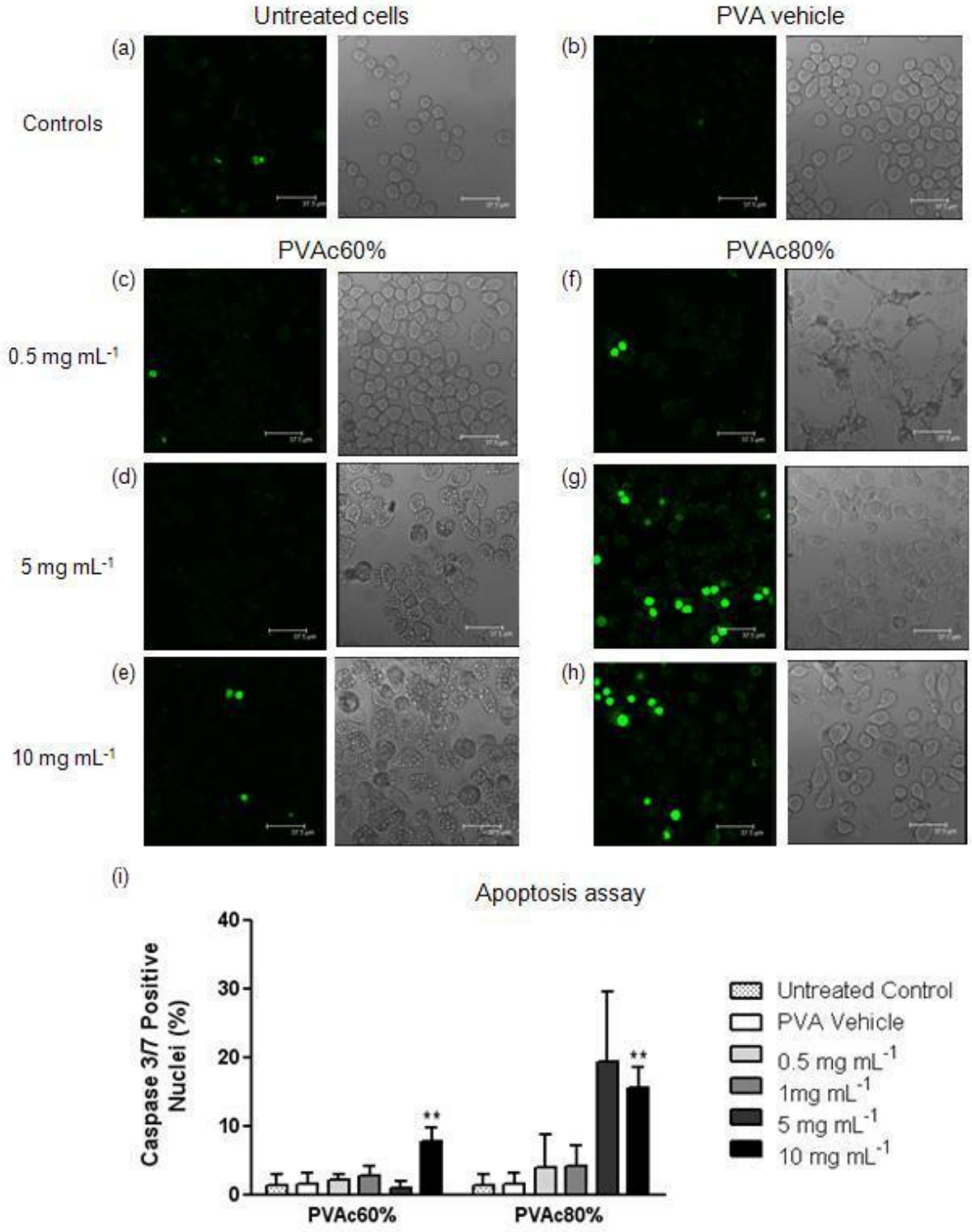
Untreated cells
PVA vehicle
(a)
(b)
Controls
PVAc60%
PVAc80%
(c)
(f)
0.5 mg mL-1
(d)
(g)
5 mg mL-1
(e)
(h)
10 mg mL-1
(i)
Apoptosis assay
Caspase 3/7 Positive Nuclei (%)
40
30
20
10
0
**
**
PVAc60%
PVAc80%
Untreated Control
PVA Vehicle
0.5 mg mL-1
1mg mL-1
5 mg mL-1
10 mg mL-1